Research Article

Yaning Zhang*, Fei Xu, Bingxi Li*, Yong-Song Kim, Wenke Zhao, Gongnan Xie, and Zhongbin Fu

Three phase heat and mass transfer model for unsaturated soil freezing process: Part 2 - model validation

https://doi.org/10.1515/phys-2018-0015
Received Oct 02, 2017; accepted Nov 26, 2017

Abstract: This study aims to validate the three-phase heat and mass transfer model developed in the first part (Three phase heat and mass transfer model for unsaturated soil freezing process: Part 1 - model development). Experimental results from studies and experiments were used for the validation. The results showed that the correlation coefficients for the simulated and experimental water contents at different soil depths were between 0.83 and 0.92. The correlation coefficients for the simulated and experimental liquid water contents at different soil temperatures were between 0.95 and 0.99. With these high accuracies, the developed model can be well used to predict the water contents at different soil depths and temperatures.

Keywords: Saturations; soil freezing; validation; water content; pre-melted film

PACS: 44.30.+v

***Corresponding Author: Yaning Zhang:** School of Energy Science and Engineering, Harbin Institute of Technology, Harbin, China; Department of Bioproducts and Biosystems Engineering, University of Minnesota, St. Paul, United States of America; Email: ynzhang@hit.edu.cn; Tel./Fax: +86 451 86412078
***Corresponding Author: Bingxi Li:** School of Energy Science and Engineering, Harbin Institute of Technology, Harbin, China; Email: libx@hit.edu.cn; Tel./Fax: +86 451 86412078
Fei Xu, Wenke Zhao, Zhongbin Fu: School of Energy Science and Engineering, Harbin Institute of Technology, Harbin, China
Yong-Song Kim: School of Energy Science and Engineering, Harbin Institute of Technology, Harbin, China; School of Energy Engineering, Kimchaek University of Technology, Pyongyang, Republic of Korea
Gongnan Xie: School of Marine Science and Technology, Northwestern Polytechnical University, Xi'an, China

1 Introduction

Computational methods have emerged as powerful techniques for investigating and exploring the physical and chemical phenomena and solving practical engineering problems. Based on fluid dynamics, computational fluid dynamics (CFD) methods have been widely used in studying the operation performances [1, 2], reaction mechanisms [3, 4], distribution fields [5, 6], and transfer processes [7, 8].

In 1988, the Lattice Boltzmann method (LBM) was introduced by McNamara and Zanetti [9] to overcome the drawbacks of the lattice gas cellular automata. Since then the LBM emerged as an alternative powerful computational method for solving fluid dynamics problems [10–12]. In traditional computational fluid dynamics methods, Navier-Stokes equations (NS) solve mass, momentum and energy conservation equations on discrete nodes, elements, or volumes. In other words, the nonlinear partial differential equations are converted into a set of nonlinear algebraic equations, which are solved iteratively. In LBM, the fluid is replaced by fractious particles, and these particles stream along given directions (lattice links) and collide at the lattice sites. The LBM can be considered as an explicit method, and the collision and streaming processes are local. Hence, it can be programmed naturally for parallel processing machines. Another beauty of the LBM is it can handle complex phenomena such as moving boundaries (multiphase, solidification, and melting problems), naturally, without a need to face tracing method as it is used in the traditional CFD. Due to the advantages of LBM mentioned above, LBM has been widely used for solving fluid dynamic problems [13, 14].

Recently, some models using LBM for the simulation of soil freezing have been developed [8, 15]. Generally, pre-melted temperature and fluid flow drive force (caused by ice formation) were usually not considered. If the pre-melted temperature is considered, it would be easier for a model to predict the water content at different tempera-

tures. Also, the considering of fluid flow drive force caused by ice formation gives a good prediction for water content distribution along depth in unfrozen zone.

In the first part (Three phase heat and mass transfer model for unsaturated soil freezing process: Part 1 - model development), a three-phase heat and mass transfer model using the LBM was developed for unsaturated soil freezing process. The model is based on both the Shen-Chen model and the mechanisms of heat and mass transfer in unsaturated soil freezing. The pre-melted film was taken into consideration, and the relationship between film thickness and soil temperature was used to calculate the liquid water fraction in both frozen zone and freezing fringe. The force that causes moisture migration was calculated by the sum of several interactive forces. The suction in the pre-melted film was regarded as an interactive force between the ice and water. Two kinds of resistance were regarded as a kind of body force related to the water films between the ice grains and soil grains. A block force instead of gravity was introduced to keep balance with gravity before soil freezing. This model is capable of predicting the water content distribution along soil depth and the variations in water content and temperature during soil freezing process. However, it should be evaluated using experimental data before its applications [16, 17]. Firstly, the water content distribution due to the water migration by suction force needed to be validated at different freezing times. Secondly, because of the introduction of pre-melted temperature, the water content variation with temperature needs to be validated for different soil depths and soil saturations.

Consequently, in this study, we tested the validity of the model. We compared the model predictions with the experimental results obtained from the previous studies on water content distribution along soil depth. Experiments were also developed to test the water content variations with temperature in different zones (unfrozen zone, freezing fringe and unfrozen zone).

2 Water content along soil depth

2.1 Experimental

The laboratory experiment data performed by Mizoguchi [18] in 1990 are classical, and they were cited in various studies [15, 19, 20], they were also used for the validation of our model in the prediction of water content distributions along the depth. In his research, Kanagawa sandy loam soil was used. Soil was packed in four identical cylinders which were 20 cm long with an internal diameter of 8 cm. Three specimens were used for performing freezing tests while the fourth was used to measure the initial condition. The side faces and bottom faces of the cylinders were thermally isolated. The specimens were prepared with the same initial temperature distribution (a uniform temperature of 6.7°C) and the volumetric water content was 0.33. The top faces of the specimens were set to be a fixed lower temperature of −6°C. Then the samples were divided into 1 cm slices for obtaining water content distributions after cooling for 12, 24 and 50 h.

2.2 Simulation settings

According to the experiment conditions mentioned above, the corresponding initial conditions and boundary conditions for the simulation in prediction of water content distributions along the depth were obtained. The porosity of sandy loam soil was between 0.4 and 0.5 [21], and 0.45 was adopted in the current research. the computational domain was given a uniform temperature of $T_0 = 6.7°C$, the initial water content was set to be 0.35, which was initialized by providing a density ratio of $\rho_w/\rho_a = 1.59 : 0.41$ to the fluid lattices of each phase, and the adjustment coefficient for suction force was given by $G_{fre} = 0.5$.

2.3 Results and discussion

Due to the suction of pre-melted film in the frozen front, water migrated from unfrozen zone to frozen zone. As shown in Figure 1 (a), after the soil freezing for 12 hours, the soil freezing fringe located nearly at the soil depth of 6.5 cm, the water content in the frozen zone decreased slightly along depth from 0.425 to 0.39, and then it increased from 0.29 to 0.33 (initial water content) along depth in the unfrozen zone. As shown in Figure 2 (a), after the soil freezing for 24 hours, the water content in the frozen zone varied in the range from 0.42 to 0.39 along the soil depth from 0 cm to 9 cm, and it increased from 0.27 to 0.32 with soil depth from 9 cm to 20 cm. As shown in Figure 3 (a), after the soil freezing for 50 hours, in the frozen zone with depth from 0 cm to 14 cm, the water content decreased slightly from 0.41 to 0.37, while in the unfrozen zone with depth from 14 cm to 20 cm, the water content increased from 0.25 to 0.30. The correlation coefficients between the predicted values and experimental data after freezing 12, 24 and 50 hours were 0.92, 0.83 and 0.92 as shown in Figure 1 (b), Figure 2 (b) and Figure 3 (b), respectively. The high correlation coefficients indicated that

Table 1: Characteristics of the glass particles prepared

Item	Value
Diameter of larger particle (um)	26
Diameter of smaller particle (um)	11
Dry powder density (g/cm^3)	1.316
Water content (g H_2O/g SiO_2)	0.151

the developed model can be well used to predict the water content distribution along soil depth.

3 Liquid water content variation with soil temperature

3.1 Experimental

The porous medium used in the experiments consisted of silica glass particles. Table 1 shows the basic characteristics of the sample. The particle size distribution was obtained by the mixture of larger particles with smaller particles, and the quality ratio between larger particles and smaller particles was fixed at 20:1. Porous medium with expected water content was prepared by placing the glass particles in a desiccator, dried for hours, added a certain quality of liquid water according to the expected quality ratio between water and glass powder, and it allows the system to equilibrate for a day.

The schematic diagram of the experiment apparatus is shown in Figure 4. The whole experimental apparatus consists of a cooling system, a sampler, three sensors and a water tank. The sampler is an important part, as shown in Figure 5. To help the sensors move with the reconstruction and frost heave, the sensors were inserted into the soil through the hole in slider blocks, the slider blocks were stacked together along the slip way, so that, the sensors can move up and down freely, and at the same time, as shown in Figure 5, due to the special geometry of slider blocks, the slider blocks can also keep the sampler sealed.

The sensors used were temperature and water content coupled meters (5TE, Decagon devices, Washington, DC, USA), The accuracy for measurement of soil volumetric water content (VWC) by Decagon device 5TE was ± 0.03 m^3/m^3, while the resolution was 0.0008 m^3/m^3 (0.08% VWC) from 0 to 50% VWC. The value of water content was gained by the indirect measurement of permittivity of soil. The sensors use capacitance to measure the dielectric permittivity of the surrounding medium. The volume of water in the total volume of soil significantly influences the dielectric permittivity of the soil because the dielectric of water is much greater than the other constituents of soil (mineral soil, $\epsilon_s = 4.15$; air, $\epsilon_a = 0.99$; ice, $\epsilon_i = 3.27$). Thus, when the amount of water changes in the soil, the sensors will measure a change in capacitance (from the change in dielectric permittivity) which can be directly correlated with a change in the water content.

The relationship between permittivity and temperature for various water contents needs to be calibrated, and the calibration curves are shown in Figure 6. It is observed that, the permittivity decreased gradually when the temperature dropped from a high temperature to a temperature near the bulk water freezing point, which was caused by the increasing water permittivity with decreasing temperature when temperature was above freezing point. Then, when the temperature passed the bulk water freezing point due to the formation of ice, the permittivity dropped rapidly. Finally, the permittivity decreased gradually again after passing the bulk water freezing point, which was caused by the decreasing ice permittivity with decreasing temperature.

The relationship between water content and soil permittivity is [22]:

$$\theta = \sqrt{\rho_w s D_a \frac{(\epsilon_r - \epsilon_a) - \theta_s(\epsilon_s - \epsilon_a)}{\epsilon_{bw} - \epsilon_i}} \quad T > 0^\circ\mathrm{C} \tag{1a}$$

$$\theta = \sqrt{\rho_w s D_a \frac{(\epsilon_r - \epsilon_a) - \theta_s (\epsilon_s - \epsilon_a) - \theta_{tot} (\epsilon_i - \epsilon_a)}{\epsilon_{bw} - \epsilon_i}} \quad T < 0^\circ\mathrm{C} \tag{1b}$$

where θ is the calculated water content, ϵ_r is the measured permittivity of soil, ρ_w is the water density, $s$is the specific surface area which is about 119.5 m^2/g, D_a is a length in which the surface force will influence the water permittivity. According to the van der Waals force, which affects dielectric properties of the media, it is steeply decreased from soil surface to about 5 nm, then it gradually decreased in the range of dozens nm [23]. In some models, the dielectric properties of water drastically changed in the length from the surface to 3-10 nm and asymptotically approached to those of bulk water [24, 25]. Here, based on the van der Waals force, we assume $D_a = 5$ nm. ϵ_{bw} is the water permittivity, and it can be calculated as:

$$\epsilon_{bw} = 88.216 - 0.4701T + 0.0024T^2 - 3 \times 10^{-5} T^3 \tag{2}$$

The calculated water content based on the permittivity was compared with the initial water content, a good agreement was observed between them, and the values are shown in Figure 7.

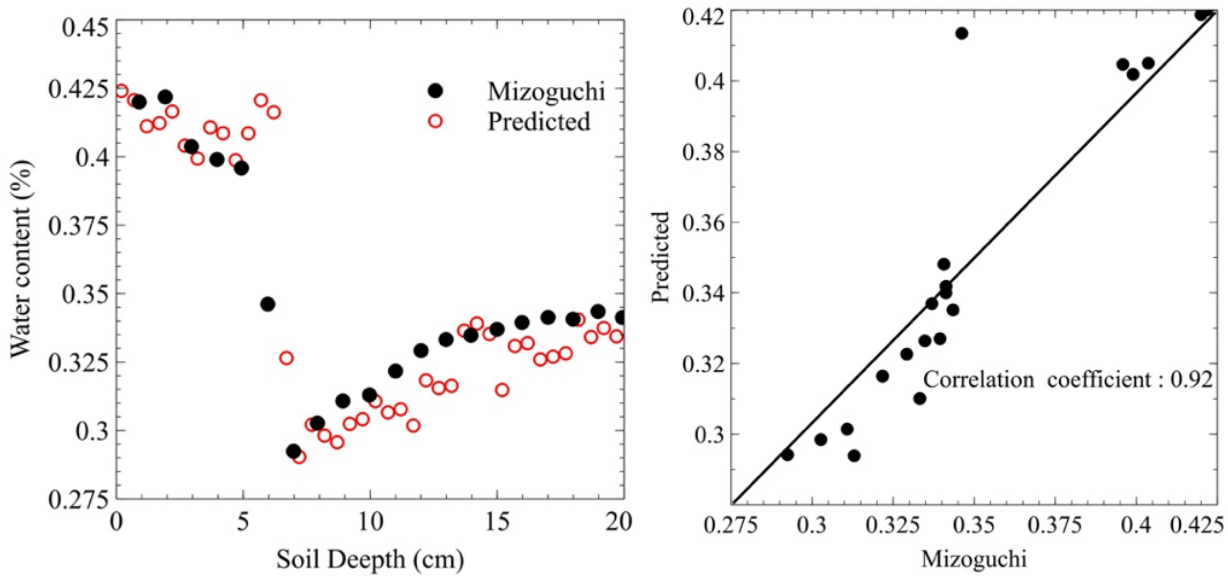

(a) Volumetric water content distribution **(b)** Correlation coefficient

Figure 1: Experimental and numerical results of water contents after 12 h freezing

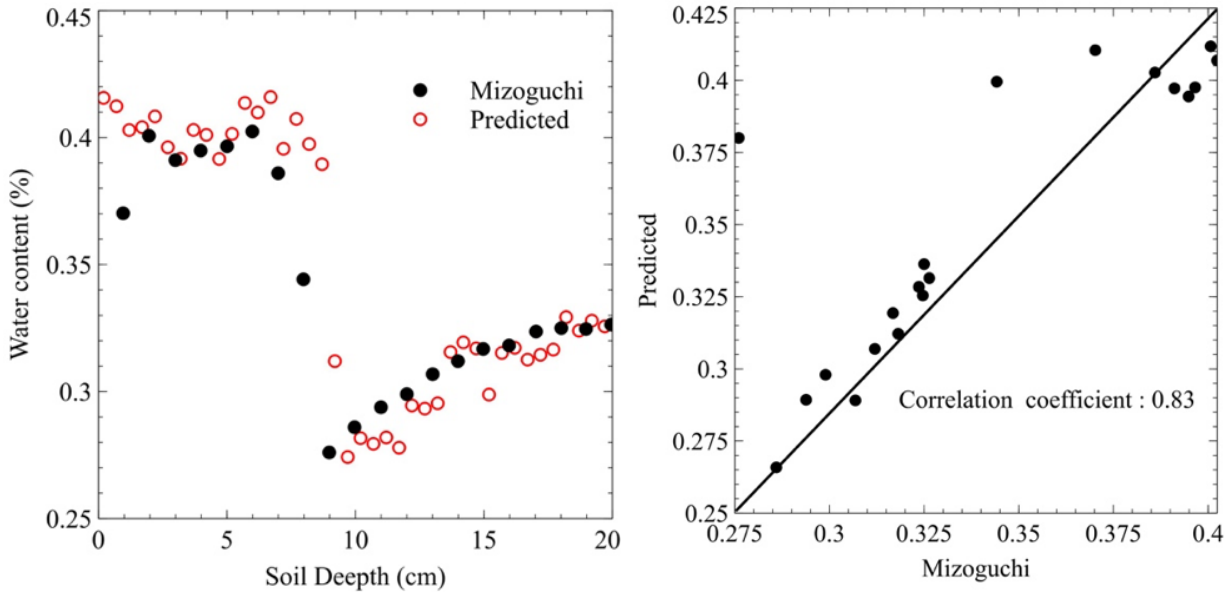

(a) Volumetric water content distribution **(b)** Correlation coefficient

Figure 2: Experimental and numerical results of water contents after 24 h freezing

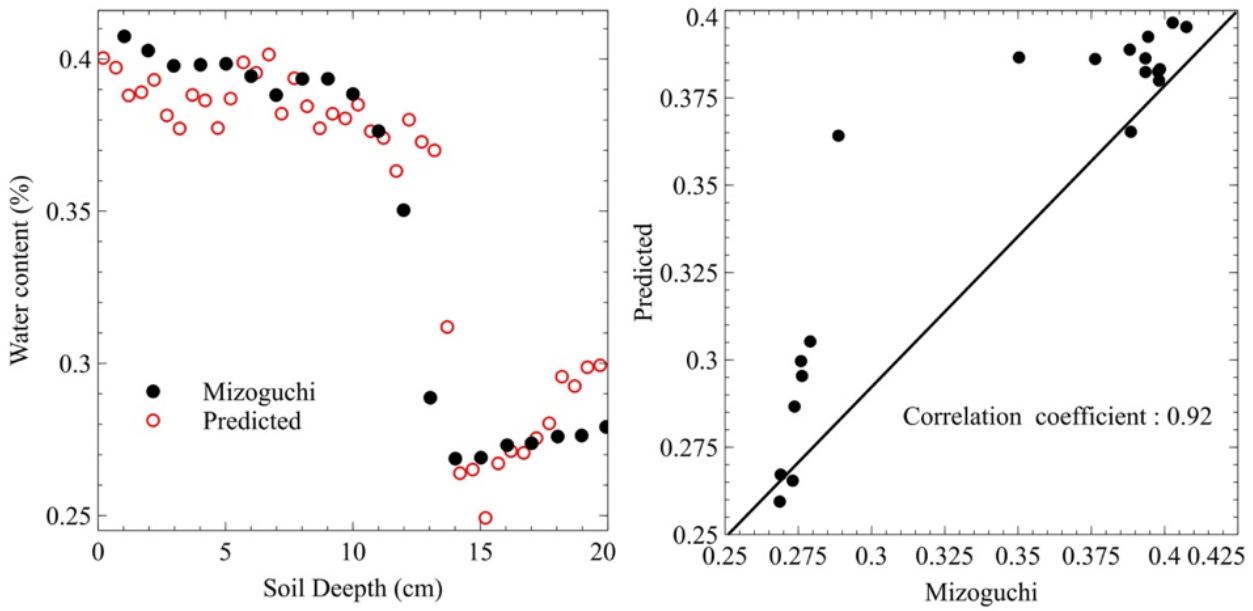

(a) Volumetric water content distribution **(b)** Correlation coefficient

Figure 3: Experimental and numerical results of water contents after 50 h freezing

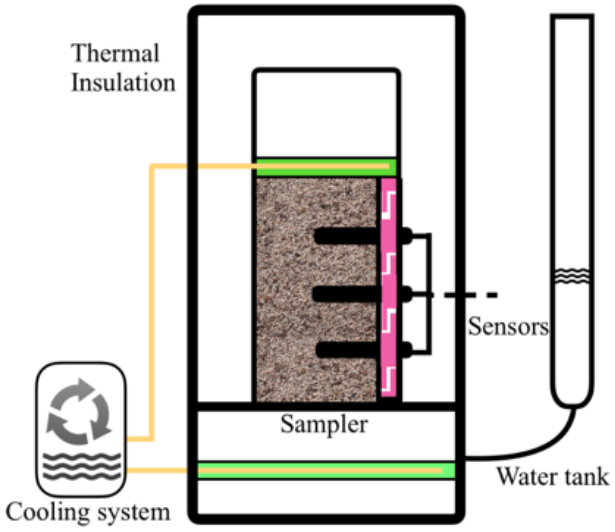

Figure 4: Soil freezing system

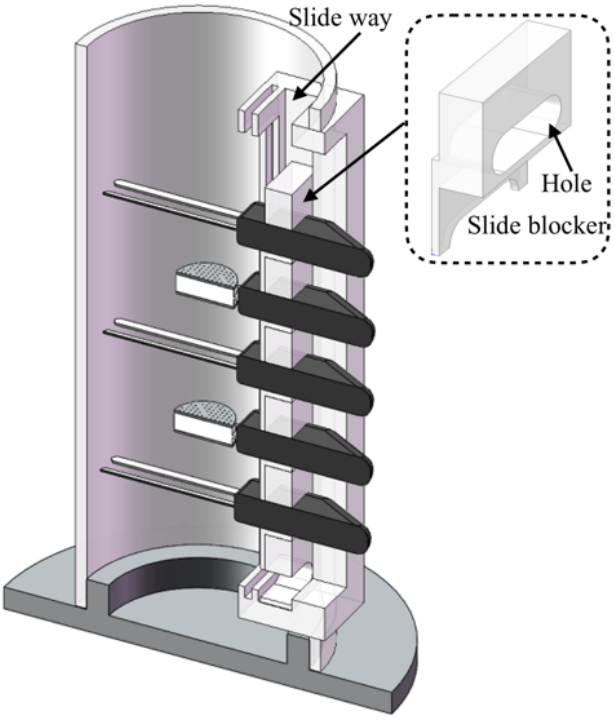

Figure 5: Sampler

The prepared sample was placed into the sampler with an inner diameter of D = 50 mm and a height of H = 200 mm, three temperature-moisture coupled sensors were inserted into the sample through the hole in slider blocks from side of the sampler with an interpret of 300 mm. The sampler was then put into a temperature gradient device, and the temperature gradient can be controlled by the up and down cooling system. Initially, the top and down walls of sampler were set to the high temperature (278 K) for two days. Then, the top wall of the sampler was set at a fixed low temperature (258 K). The temperature and liquid wa-

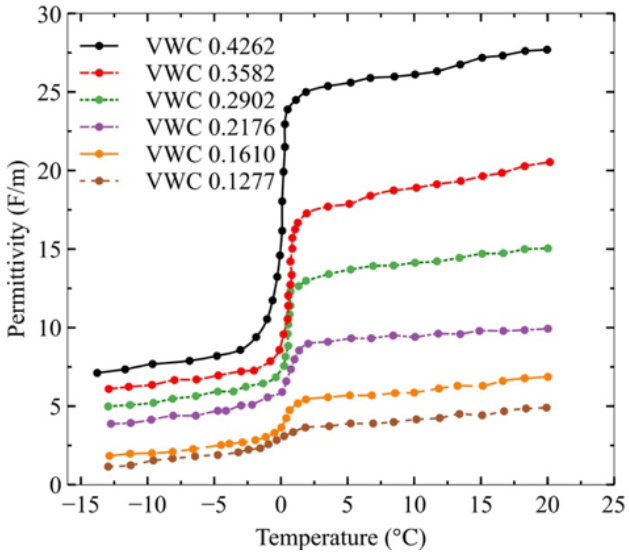

Figure 6: Calibration curve under various soil water contents

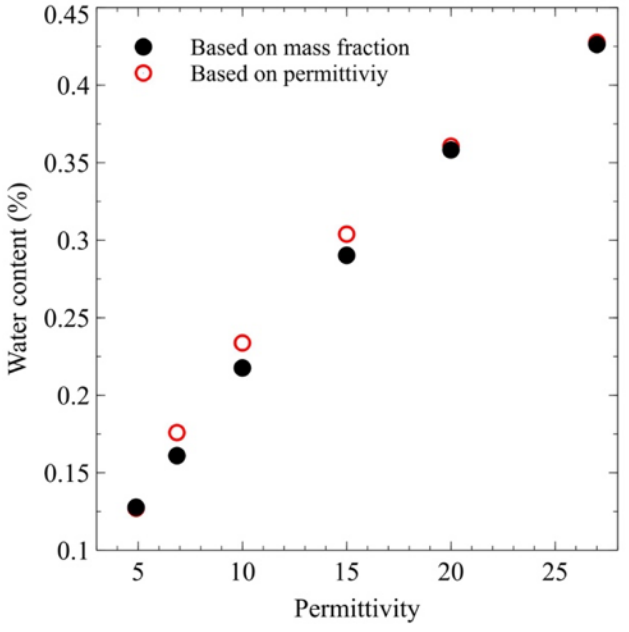

Figure 7: Water contents at different permittivities

ter content of each test point were recorded at 20 min intervals.

3.2 Simulation settings

In the simulation of water content at different temperatures with soil saturation of 0.32 and 0.16, based on the experiment conditions mentioned above, the corresponding initial conditions and boundary conditions were given. 0.45 was adopted for the porosity of sandy loam soil. The computational domain was given a uniform temperature of $T_0 = 5°C$, providing density ratios of $\rho_w/\rho_a = 1.46 : 0.54$ and $\rho_w/\rho_a = 0.73 : 1.27$ for soil saturation of 0.33 and 0.16, respectively. The adjustment coefficient for suction force is given by $G_{fre} = 1.5$.

3.3 Results and discussion

The experimental data of liquid water content variation with temperature were obtained from the experiments conducted in this study. The liquid water contents and soil temperatures were measured simultaneously at two points for soils with two kinds of saturation (0.33, 0.16). The first point was 30 mm away from the top (up) wall, and the interpret between the two points was 30 mm.

For the soil with saturation of 0.33, the experimental and numerical results of liquid water contents at different temperatures are shown in Figure 8. Due to the temperatures of the top and bottom walls, which were fixed at 258 K and 278 K, respectively, a temperature gradient from the bottom to the top was formed, and this temperature gradient caused a heat flow coupled with water migration during the soil freezing process. When the temperature decreased from 278 K to the freezing point due to the suction of freezing fringe, the liquid water content decreased gradually from the initial value to about 0.30 for both point 1 and point 2. When the temperature decreased from the freezing point to 268 K, the liquid water content decreased rapidly due to the freezing of pore water, then, the liquid water content decreased gradually due to the formation of pre-melted film. In the temperature variation range from

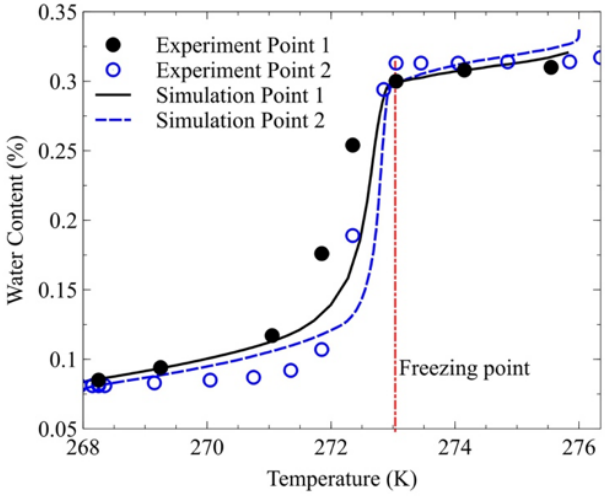

Figure 8: Simulated and experimental liquid water contents at different soil temperatures (initial saturation is 0.33)

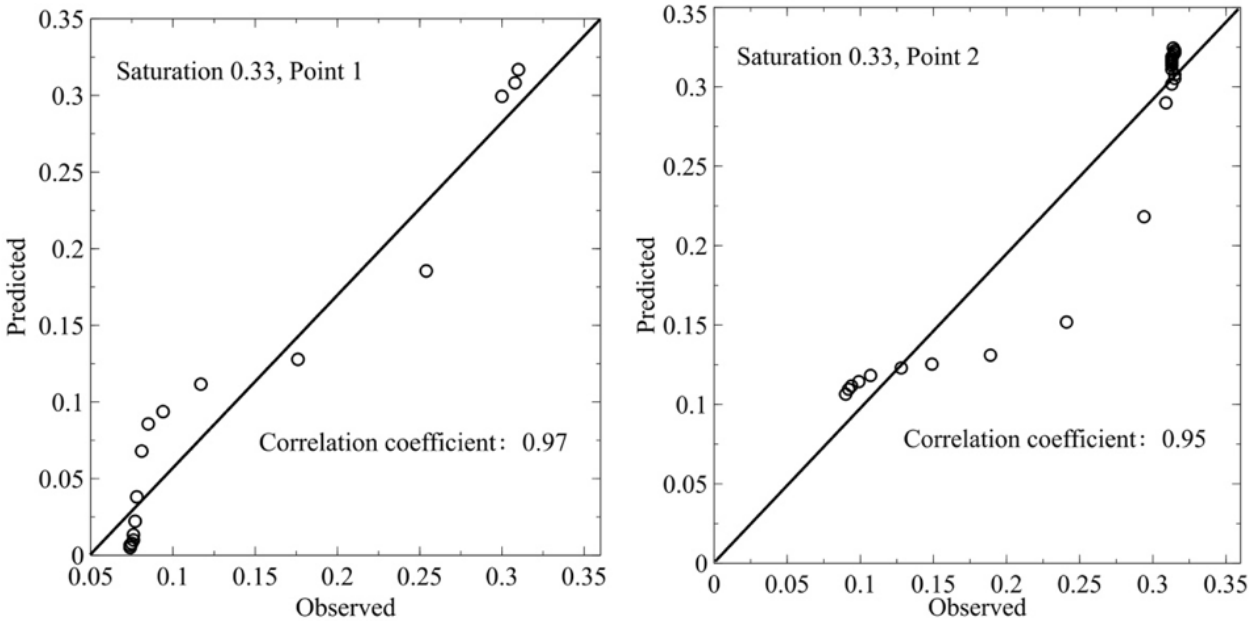

(a) point 1 **(b)** point 2

Figure 9: Correlation coefficients for simulated and experimental liquid water contents (initial saturation is 0.33)

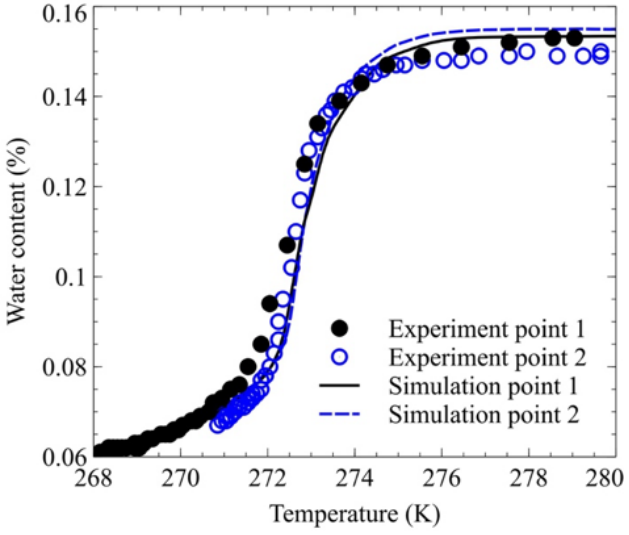

Figure 10: Simulated and experimental liquid water contents at different soil temperatures (initial saturation is 0.16)

278 K to 258 K, the liquid water content decreased from 0.33 to 0.08 in both experimental and numerical results. The correlation coefficients of the predicted and observed liquid water contents were 0.97 and 0.95 for point 1 and point 2, respectively, as show in Figure 9. These high accuracies may be attributed to (a) the consideration of pre-melted film, and the existence of pre-melted film permitted the unfrozen water in the frozen zone, and (b) the lower freezing point of water in thinner pre-melted film, and this relationship made the liquid water content decrease gradually with soil temperature in the frozen zone. What's more, according to Figure 8, the decrease in liquid water content at point 2 was a little fast than that at point 1, this was caused by the different temperature gradients in the freezing fringe.

For the soil with saturation of 0.16, the experimental and numerical results of liquid water contents at different temperatures are shown in Figure 10. The liquid water content variations were similar to those of soil with saturation of 0.33. When the temperature decreased from 278 K to the freezing point, the liquid water content decreased gradually from the initial value to about 0.14 for both point 1 and point 2. When the temperature decreased from the freezing point to 268 K, the liquid water content decreased, then, gradually to 0.06. Figure 11 shows the correlation coefficients of the predicted and measured liquid water contents. It is observed that the correlation coefficients are 0.99 for both point 1 and point 2, indicating that the developed model can be well used to predict the liquid water contents at different soil temperatures.

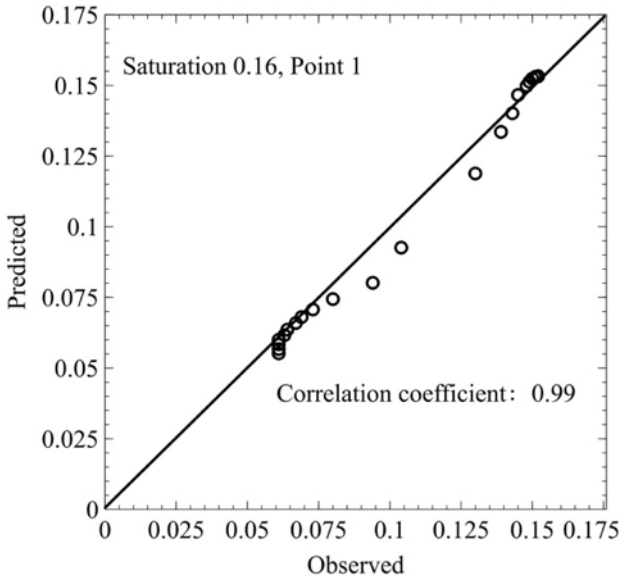

(a) point 1

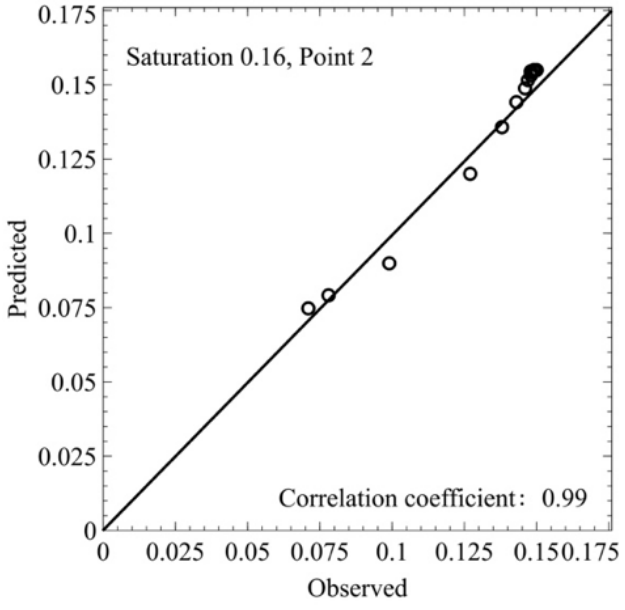

(b) point 2

Figure 11: Correlation coefficients for simulated and experimental liquid water contents (initial saturation is 0.16)

4 Conclusions

The water contents at different soil depths and temperatures were used to validate the model developed in the first part. Some conclusions were obtained.

The simulated and experimental water contents at different soil depths varied in the ranges of 0.425-0.26 and 0.425-0.25, respectively, and the correlation coefficients were between 0.83 and 0.92.

For the soil saturation of 0.33, when the temperature decreased from 278 K to 258 K, both the simulated and experimental water contents at different soil depths ranged in 0.33-0.08, and the correlation coefficients were between 0.95 and 0.97.

For the soil saturation of 0.16, when temperature decreased from 278 K to 258 K, both the simulated and experimental water contents at different soil depths ranged in 0.16-0.06, and both the correlation coefficients were 0.99.

The developed model can be well used to predict the water contents at different soil depths and temperatures.

Acknowledgement: This study is supported by Natural Science Foundation of China (Grant NO. 51776049), Special Foundation for Major Program of Civil Aviation Administration of China (Grant No. MB20140066) and National Materials Service Safety Science Center open fund.

Nomenclature

θ calculated water content (dimensionless)
S specific surface area (m^2/m^3)
T temperature (K)
G^{fre} parameter control the suction force between ice and fluids (dimensionless)
D_a a length in which the surface force will influence the water permittivity (nm)
$\boldsymbol{D}$ inner dimeter of sampler (mm)
$\boldsymbol{H}$ height of sampler (mm)

Subscripts

i ice
a air
w water
s solid

References

[1] Xu Z., Zhang Y., Li B., Wang C.C., Ma Q., Heat performances of a thermosyphon as affected by evaporator wettability and filling ratio, Applied Thermal Engineering, 2018, 129, 665-673.
[2] Xu Z., Zhang Y., Li B., Wang C.C., Li Y., The influences of the inclination angle and evaporator wettability on the heat performance of a thermosyphon by simulation and experiment, Inter-

national Journal of Heat and Mass Transfer, 2018, 116, 675-684.
[3] Gao X., Zhang Y., Li B., Zhao Y., Jiang B., Determination of the intrinsic reactivities for carbon dioxide gasification of rice husk chars through using random pore model. Bioresource Technology, 2016, 218, 1073-1081.
[4] Huang X., Hong J., Zhang Y., Shuai Y., Yuan Y., Li B., Tan H., Exergy distribution characteristics of solar-thermal dissociation of $NiFe_2O_4$ in a solar reactor, Energy, 2017, 123, 131-138.
[5] Wang W., Zhang Y., Li B., Han H., Gao X., Influence of geometrical parameters on turbulent flow and heat transfer characteristics in outward helically corrugated tubes, Energy Conversion and Management, 2017, 136, 294-306.
[6] Wang W., Zhang Y., Li B., Li Y., Numerical investigation of tube-side fully developed turbulent flow and heat transfer in outward corrugated tubes, International Journal of Heat and Mass Transfer, 2018, 116, 115-126.
[7] Zhang Y., Yu X., Li B., Exergy transfer research on the Sandia Flame D - A turbulent piloted methane-air jet flame, Heat Transfer Research, 2016, 47(12), 1169-1186.
[8] Song W., Zhang Y., Li B., Xu F., Fu Z., Macroscopic lattice Boltzmann model for heat and moisture transfer process with phase transformation in unsaturated porous media during freezing process, Open Physics, 2017, 15(1), 379-393.
[9] Mcnamara G.R., Zanetti G., Use of the Boltzmann equation to simulate lattice gas automata, Physical Review Letters, 1988, 61(20), 2332.
[10] Guo Z., Shu C., Lattice Boltzmann Method and Its Applications in Engineering. 2013, World Scientific Publishing Co. Ltd., Singapore
[11] Huang H., Sukop M.C., Lu X., Multiphase Lattice Boltzmann Methods: Theory and Application, 2015, 1-17.
[12] Krüger T., Kusumaatmaja H., Kuzmin A., Shardt O., Silva G., Viggen E.M., The Lattice Boltzmann Method - Principles and Practice, 2017
[13] Kotapati R., Keating A., Kandasamy S., Duncan B., Shock R., Chen H., The Lattice-Boltzmann-VLES Method for Automotive Fluid Dynamics Simulation, a Review, 2009, DOI: 10.4271/2009-26-0057
[14] Luo L.H., Krafczyk M., Shyy W., Lattice Boltzmann Method for Computational Fluid Dynamics, John Wiley & Sons, Ltd., 2010
[15] Song W., Zhang Y., Li B., Fan X., A lattice Boltzmann model for heat and mass transfer phenomena with phase transformations in unsaturated soil during freezing process, Int. J. of Heat and Mass Transf., 2016, 94, 29-38.
[16] Xu Z., Zhang Y., Li B., Huang J., Modeling the phase change process for a two-phase closed thermosyphon by considering transient mass transfer time relaxation parameter, Int. J. of Heat and Mass Transf., 2016, 101, 614-619.
[17] Gao X., Zhang Y., Li B., Yu X., Model development for biomass gasification in an entrained flow gasifier using intrinsic reaction rate submodel, Energy Conversion and Management, 2016, 108, 120-131.
[18] Mizoguchi M., Water Heat and Salt Transport in Freezing Soil, University of Tokyo, Tokyo, 1990
[19] Hansson K., Simunek J., Mizoguchi M., Lundin L.C., van Genuchten M.T., Water flow and heat transport in frozen soil: Numerical solution and freeze-thaw applications, Vadose Zone Journal, 2004, 3(2), 693-704.
[20] Tan X., Chen W., Tian H., Cao J., Water flow and heat transport including ice/water phase change in porous media: Numerical simulation and application, Cold Regions Science and Technology, 2011, 68(1-2), 74-84.
[21] Shahid S.A., Qidwai A.A., Anwar F., Ullah I., Rashid U., Improvement in the water retention characteristics of sandy loam soil using a newly synthesized poly (acrylamide-co-acrylic acid)/$AlZnFe_2O_4$ superabsorbent hydrogel nanocomposite material, Molecules, 2012, 17(8), 9397- 9412.
[22] Watanabe K., Wake T., Measurement of unfrozen water content and relative permittivity of frozen unsaturated soil using NMR and TDR, Cold Regions Science and Technology, 2009, 59(1), 34-41.
[23] Israelachvili J.N., Intermolecular and Surface Forces - Intermolecular and Surface Forces (Third Edition), Quarterly Review of Biology, 2010, 2(3), 59-65.
[24] Or D., Wraith J.M., Temperature effects on soil bulk dielectric permittivity measured by time domain reflectometry: A physical model, Water Resources Research, 1999, 35(7), 2283-2283.
[25] Boyarskii D.A., Tikhonov V.V., Komarova N.Y., Model of dielectric constant of bound water in soil for applications of microwave remote sensing - Abstract, Journal of Electromagnetic Waves and Applications, 2002, 16(3), 411-412.